IJE TRANSACTIONS B: Applications Vol. 34, No. 05, (May 2021) 1352-1361

International Journal of Engineering

Journal Homepage: www.ije.ir

Influence of Immersion Corrosion on Mechanical Properties of AISI 430/AISI 316L Dissimilar Welded Joints

A. M. Barrios[a], L. M. Burgos[a], E. E. Niebles-Nuñez[b], L. A. Espitia[a], J. Unfried-Silgado*[a]

[a] *Department of Mechanical Engineering, ICT research group, Universidad de Córdoba, Montería, Colombia*
[b] *Mechanical Engineering Program, IMTEF research group, Universidad Autónoma del Caribe, Barranquilla, Colombia*

PAPER INFO

Paper history:
Received 10 February 2021
Received in revised form 27 March 2021
Accepted 30 March 2021

Keywords:
Dissimilar Welded joints
Stainless Steel
Corrosion
Tensile Test
Heat-affected Zone

ABSTRACT

Dissimilar welded joints of AISI 430 and AISI 316L stainless steel were produced by the GMAW process using two different shielding gas mixtures composed of 97Ar-3N_2 and 80Ar-19He-1O_2. The microstructure of the heat-affected zone was characterized by optical and scanning electron microscopy, and Vickers microhardness measurements were carried out along the cross-section of the specimens. The dissimilar welded joints were submitted to immersion corrosion test in a 10%v/v hydrochloric acid solution for 24 and 72 hours. Afterward, yields strength, tensile strength, and elongation percentage were measured using tensile tests according to ASTM E8 standard. Non-immersed welded joints were used for comparison purposes. An analysis of variance was developed to evaluate the influence of immersion time and shielding gas mixture on yielding strength and tensile strength. The microstructure characterization showed that the heat-affected zone on AISI 430 side was the widest, and it was observed a significant presence of acicular ferrite, martensite, and coarsened ferritic grains. In contrast, on the heat-affected zone on AISI 316L side was not observed coarsening nor refinement of austenite grains. The AISI 430 heat-affected zone showed the maximum hardness values and higher susceptibility to corrosion damage. Tensile tests results evidenced that immersion corrosion tests did not change significantly ultimate strength in comparison to non-immersed specimens while yielding strength and elongation percentage were drastically decreased due to immersion time. According to the p-value, the immersion time is the most influencing factor on yielding strength and tensile strength of the dissimilar welded joints.

***doi**: 10.5829/ije.2021.34.05b.31*

NOMENCLATURE

Sy	Yield Strength	LF-A	Fusion line on the austenitic side
UTS	Ultimate Tensile Strength	HAZ-F	Heat-affected zone on the ferritic side
ε%	Elongation Percentage	HAZ-A	Heat-affected zone on the austenitic side
LF-F	Fusion line on the ferritic side		

1. INTRODUCTION

Dissimilar welded joints have been extensively employed in industrial applications where different combination of mechanical, chemical, and physical properties are required. Several parts of machinery and devices used in pharmaceutical, petrochemical, food processing, and mining industries make use of dissimilar welded joints, where functional combinations of high tensile strength, high corrosion resistance, and cost reductions with maximum performance on service are mandatory [1-3]. Typical metallic dissimilar welded joints in industrial applications are composed of carbon steel/stainless steel, stainless steel/nickel alloys, cooper alloys/carbon steels, aluminum alloys/galvanized steel alloys, among others [4-8]. To achieve a balance among chemical composition, microstructure, and properties, some special welding techniques are used. The most

*Corresponding Author Institutional Email: *jimyunfried@correo.unicordoba.edu.co* (J. Unfried-Silgado)

Please cite this article as: A. M. Barrios, L. M. Burgos, E. E. Niebles-Nuñez, L. A. Espitia, J. Unfried-Silgado, Influence of Immersion Corrosion on Mechanical Properties of AISI 430/AISI 316L Dissimilar Welded Joints, International Journal of Engineering, Transactions B: Applications Vol. 34, No. 05, (2021) 1352-1361

representative techniques for obtaining dissimilar welding joints include buttering, using a third metal or a filler metal different to base metals, prefilling, among others [9-11]. Particularly, dissimilar austenitic/ferritic stainless steels welded joints due to the low susceptibility of stress corrosion cracking of AISI 430 and the high corrosion resistance and weldability of AISI 316L are a remarkable choice when these conditions are required [12-14]. Rajput el al. [15] indicated that one of the major problems ocurring in dissimilar welded joints of austenitic/ferritic stainless steels is the hot corrosion cracking ocurring on the austenitic side in chloride enviroments. Unlike, ferritic stainless steels showed good stress corrosion cracking resistance and pitting corrosion resistance. Nevertheless, it is widely accepted that ferritic stainless steels exhibit less corrosion resistance than austenitic stainless steels. Additionally, phase transformations of these dissimilar welded joints have been extensively investigated. Both ferritic and austenitic stainless plates of steels may undergo coarsening and refinement of grain at different regions, as well as, several phase transformations along the heat-affected zone [16-18]. All these metallurgical changes may modify the corrosion behavior of welded joints and they are functions of several factors, such as the as-received condition of base metals, shielding gas mixtures, thermal cycling, heat input, temperatures, and cooling rates imposed during the welding process. The corrosion behavior of stainless steels has been evaluated using potentiostatic and potentiodynamic tests [18-20], stress corrosion cracking tests (SCC) [21], and in few cases, using immersion corrosion tests [22]. Corrosion behavior on acid environments of dissimilar welded joints of stainless steels [19, 20-22], and tensile and microstructural properties of welded joints of different grades of austenitic stainless steels [23] have been evaluated by several authors. For instance, Maheswara and Srinivasa [24] evaluated the pitting corrosion of AISI 304/AISI 430 dissimilar welded joints exposed to NaOH, NaCl, and HCl solutions. It was reported that the fusion zone showed higher corrosion damage compared to the heat-affected zone due to the higher heat input and the chromium depletion at this area during the welding process. However, the characterization carried out in those works was focused on small regions of the welded joints, which makes it difficult to establish correlations between corrosion behavior and mechanical properties of the entire joint. These relationships are especially important to understand the behavior of dissimilar welded joints exposed to aggressive acid environments during service. These relationships might be achieved using design and analysis of experiments such as the analysis of variance (ANOVA) [25-26]. In this work, the influence of immersion corrosion in hydrochloric acid solution on microstructure, corrosion resistance, and mechanical properties of AISI 430/AISI 316L dissimilar welded joints was assessed, and the effect of process parameters and corrosion immersion time on mechanical properties was determined using the ANOVA model.

2. MATERIALS AND METHODS

2. 1. Materials and welding procedure

Commercial AISI 430 and AISI 316L stainless steel plates were used in this work. Table 1 showed the nominal [27] and the measured chemical composition of the steels determined by optical emission spectrometry.

Dissimilar welded joints were fabricated from workpieces of 400 x 200 x 3 mm using a square butt joint and gas metal arc welding (GMAW) process. Table 2 shows the process parameters, the shielding gas mixtures, and the heat inputs used to obtain two dissimilar welded joints referred to from this point on as GA and GB specimens.

The welding processes were carried out in a single pass at the flat position with a commercial ER309L rod wire as filler metal. Table 3 shows the nominal chemical composition of the AWS ER309L electrode [28].

TABLE 1. Nominal [27] and measured chemical composition of the stainless steels. N: Nominal. M: Measured

Material		Fe	C	Si	Mn	Cr	Ni	Mo	S	P
AISI 430	N	Bal.	0.12 max	1.0 max	1.0 max	16.0 – 18.0	0.75 max	0.60 max	0.030 max	0.040 max
	M	Bal.	0.019	0.245	0.377	16.07	0.225	0.055	0.03	0.01
AISI 316L	N	Bal.	0.030 max	0.75 max	2.00 max	16.0 – 18.0	10.0 – 14.0	2.0 – 3.0	0.030 max	0.045 max
	M	Bal.	0.027	0.275	1.748	17.08	9.758	1.2	0.01	0.03

TABLE 2. Welding process parameters

Dissimilar welded joints	Shielding gases mixture	I (A)	V (V)	Average Heat Input (kJ.cm^{-1})	Welding speed (mm.s^{-1})
GA	97Ar - 3N_2	130.5	22.5	3.2	5.7
GB	80Ar - 19He - 1O_2	140.5	22.8	2.8	7.3

TABLE 3. Nominal chemical composition of the ER309L wire rode electrode [28]

Element	C	Cr	Ni	Mo	Mn	Si	P	S	Cu
wt%	0.03 max	23.0 – 25.0	12.0 – 14.0	0.75 max	1.0 – 2.5	0.30 – 0.65	0.03 max	0.03 max	0.75 max

2. 2. Microstructure Characterization and Hardness Measurements Cross-section specimens with 50 mm length were extracted from the steady region of each welded joint and then mounted in epoxy resin for microstructure characterization and microhardness measurements, as shown in Figure 1.

Cross-section specimens were ground with emery papers and polished with 1 μm alumina particles. The microstructure was revealed using aqua regia reagent during 15 s according to ASTM E407 standard [29], and subsequently examined by stereoscopic microscopy, optical microscopy, and scanning electron microscopy. Vickers microhardness measurements before and after the corrosion tests were carried out along the cross-section of specimen length using a 500 g load during 10 s according to ASTM E384 standard [30], as illustrated in Figure 1c. Schaeffler diagram was used to predict microstructure of the fusion zone, and subsequently, to assess its susceptibility to corrosion damage. Chromium and Nickel equivalent was calculated using equations 1 and 2, employing the chemical composition of the electrode, base metals and assuming a 43 % dilution at the fusion zone, as suggested in similar works [33-35].

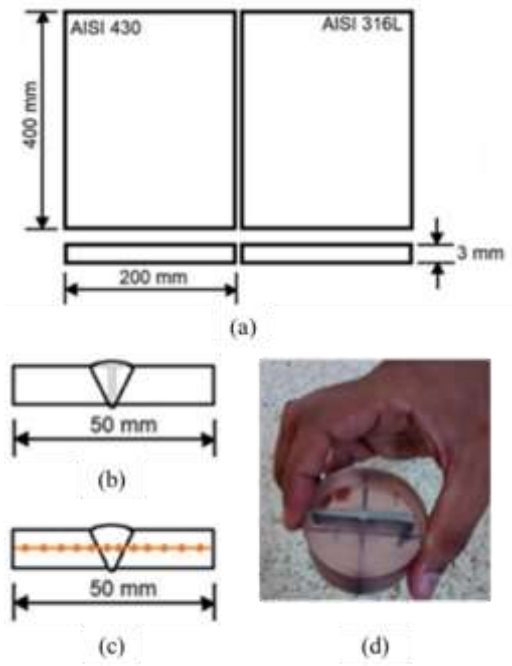

Figure 1. (a) Schematic of dissimilar welded joint (b) Schematic of cross-section specimen. (c) Microhardness measurements profile. (d) Specimen for microhardness measurements

$$Creq = Cr + Mo + 1.5Si + 0.5\,Nb \quad (1)$$

$$Nieq = Ni + 30C + 0.5\,Mn \quad (2)$$

2. 3. Tensile and Corrosion Immersion Tests Flat tensile specimens according to ASTM E8 standard [31] were manufactured from the 3 mm thick dissimilar welded joint using a water jet cutter as shown in Figure 2. The specimens were ground until 600 emery paper and the welded joint was perpendicular to the rolling direction.

Corrosion immersion tests were carried out in a 10%v/v hydrochloric acid solution according to practice C of ASTM A262-02 standard [32]. GA and GB specimens were completely submerged into the HCl solution during 24 and 72 hours at 303 K.The specimens were isolated from environmental contaminants, as shown in Figure 3. Temperature, humidity, and pH of the solution were continuously controlled during the tests. Specimens mass was measured before and after the tests using a scale with 0.01 mg resolution.

Tensile tests were carried out in a 300 kN MTS Criterion C45.305 universal machine using a testing speed of 0.06 mm s^{-1}. Yield Strength (Sy), Ultimate Tensile Strength (UTS), and Elongation Percentage (ε%) were calculated from stress-strain diagrams. Non immersed welded joints, together with AISI 430 and AISI 316L stainless steels in the as-received condition were used for comparison purposes. The results are the average of four random tests performed under the same conditions. Furthermore, an analysis of variance (ANOVA) was carried out to evaluate the effect of immersion time and shielding gas type on Sy and UTS.

The experiment was conducted at three levels of immersion time (0h, 24 h, and 72 h), two levels of shielding gas type (97Ar - $3N_2$ and 80Ar - 19He - $1O_2$), and four replicates for each condition. The effect

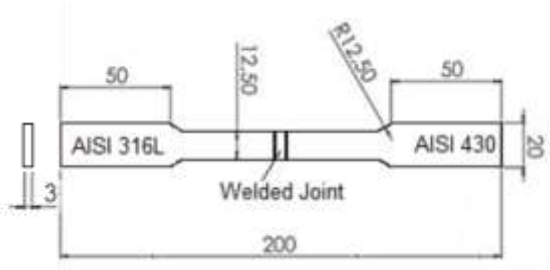

Figure 2. Flat tensile specimens according to ASTM E8 standard. Dimensions in mm [32]

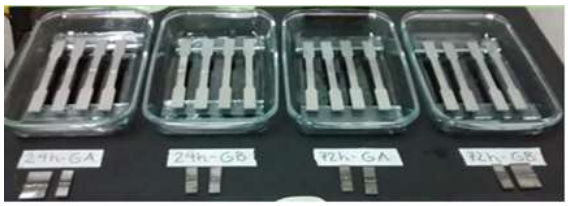

(a) Immersed specimens.

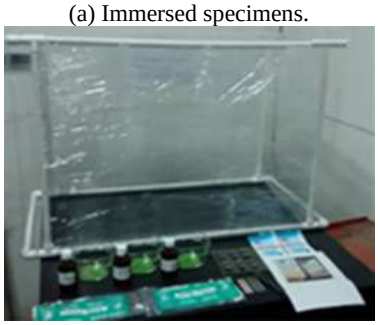

(b) Isolation Chamber

Figure 3. Immersion corrosion tests setup

estimation was carried out using a randomized block design, the classical sum of squares - type II, and a 95 % confidence interval.

3. RESULTS AND DISCUSSION

Figure 4 shows the microstructure of AISI 430 and AISI 316L stainless steels in the as-received condition.

Both materials showed ferrite and austenite grains, the typical microstructure of ferritic and austenitic stainless steels, with an average microhardness of 150 ± 6 HV1kgf and 158 ± 6 HV1kgf, respectively. Considering the hardness, size, and shape of the grains, and the twins in AISI 316L microstructure, it is assumed that the stainless steels were annealed after cold rolling.

Figures 5, 6, and 7 show the appearance and microstructure characteristics of GA and GB specimens in the non-immersed condition and after corrosion immersion tests. The welded joints were free of weld defects such as cracking and porosity.

Length and microstructure on HAZ of GA and GB specimens were strongly influenced by welding

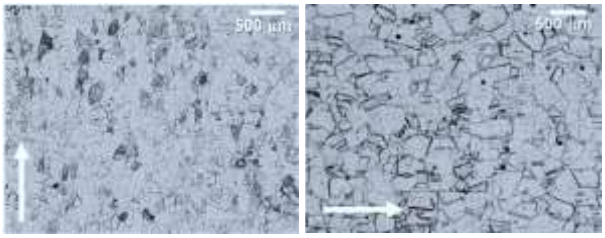

(a) (b)

Figure 4. The microstructure of the stainless steels in the as-received condition, a) AISI 430 and b) AISI 316L. White arrows indicate rolling direction. OM 500x

(a) (b)

Figure 5. The appearance of GA and GB specimens in the (a) non-immersed condition and (b) after corrosion immersion tests. The welded joints were free of weld defects such as cracking and porosity

processes. HAZ-F length on GA specimens was from 3.5 to 4.5 mm, while on GB specimens were from 2.2 to 2.5 mm. Likewise, HAZ-A length was in the range from 3.0 to 3.2 mm, and 2.0 to 2.5 mm on GA and GB specimens, respectively. These length differences on HAZ of GA and GB specimens are the consequence of welding process parameters and thermal conductivity of the stainless steels. Heat input was higher in GA specimens, therefore, a longer HAZ is expected. Moreover, thermal conductivity in ferritic stainless steels is ~ 40 % higher in comparison to austenitic stainless steels [36]. Regarding microstructure, on HAZ- F was observed coarsening of ferrite grains and presence of acicular ferrite and Martensite near to LF-F, as shown in Figure 8a. Towards to base metal, the HAZ-F microstructure showed a gradual grain refinement. On HAZ – A was not observed grain coarsening nor refinement; in fact, elongated grains structure produced by cold rolling remained unchanged. However, near to LF-A, due to the temperature and cooling rates achieved at this region during the welding process, the microstructure showed a slightly homogeneous austenitic grain size and presence of $M_{23}C_6$ carbides [16], as can be seen in Figure 8b.

On the other hand, HAZ of GA and GB specimens suffered higher corrosion damage. It was observed pitting and intergranular corrosion, mainly at HAZ-F, as shown in Figures 6c and 6d, and Figures 7c and 7d (highlighted with yellow arrows). Additionally, corrosion damage increased with immersion time. It has been reported that ferritic stainless steels exhibit lower corrosion resistance than austenitic stainless steels under similar conditions, [12, 16]. Furthermore, dissolution behavior is fastest on AISI 430 than AISI 316 stainless steel in acidic chloride solutions with ions dissolution of Fe and Cr in each stainless steel, respectively [21]. Due to heterogeneity of located corrosion, mass losses after the immersion corrosion tests were disregarded in this work.

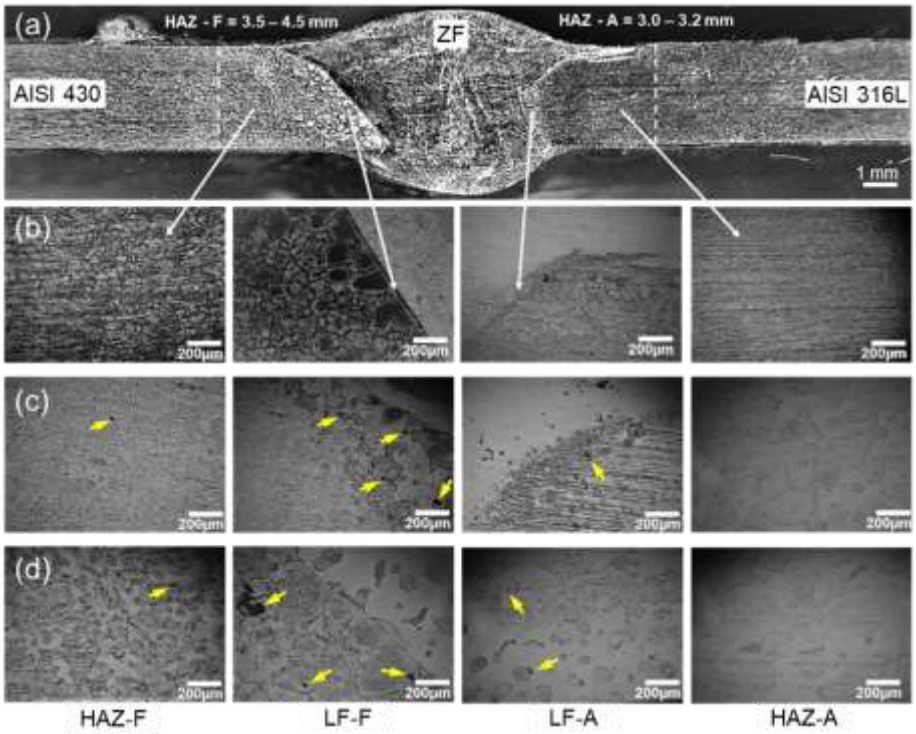

Figure 6. a) Welded joint of GA specimens, b) Non-immersed GA specimen, c) 24 hours immersed GA specimen, and d) 72 hours immersed GA specimen. HAZ-F: heat-affected zone on the ferritic side, LF-F: fusion line on the ferritic side, LF-A: fusion line on the austenitic side, HAZ-A: heat-affected zone on the austenitic side

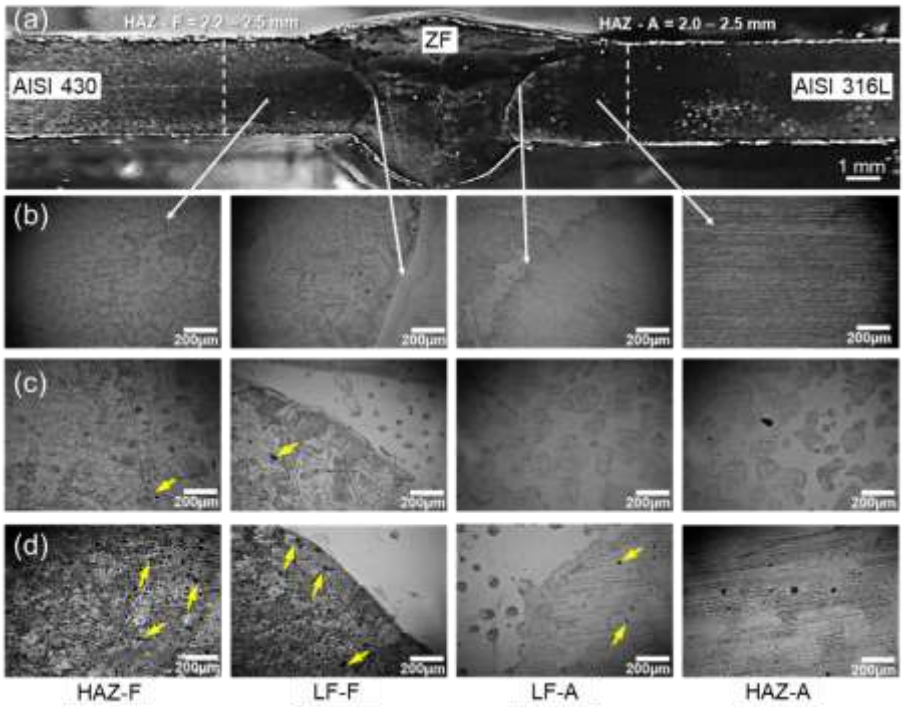

Figure 7. a) Welded joint of GB specimens, b) Non-immersed GB specimen, c) 24 hours immersed GB specimen, and d) 72 hours immersed GB specimen. HAZ-F heat-affected zone on the ferritic side, LF-F: fusion line on the ferritic side, LF-A: fusion line on the austenitic side, HAZ-A: heat-affected zone on the austenitic side

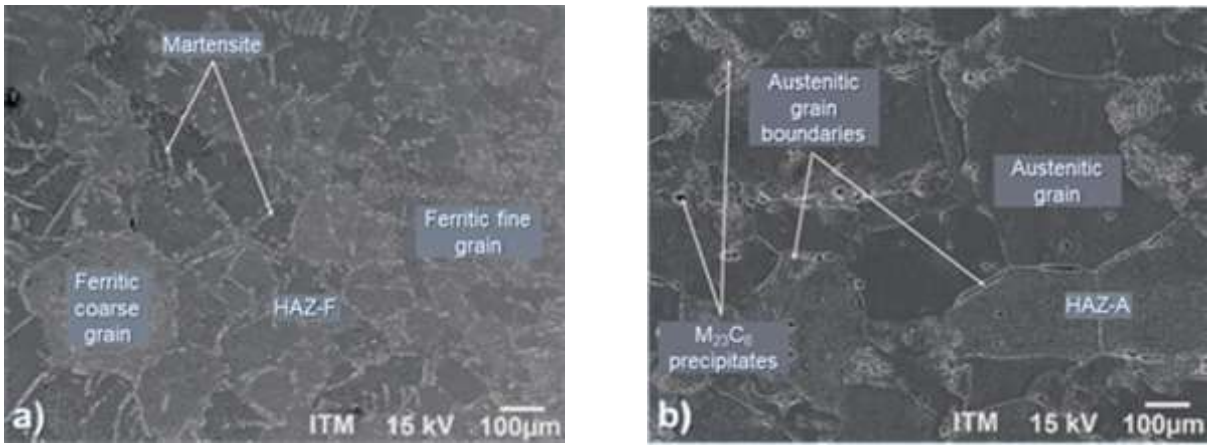

(a) (b)

Figure 8. a) Coarsened ferrite grains and presence of acicular ferrite and Martensite on HAZ- F near to LF-F, b) Homogeneous austenitic grain size and presence of M23C6 carbides on HAZ- A near to LF-A

Figure 9 shows the Vickers microhardness profile along the cross-section of GA and GB specimens before and after immersion tests. Higher microhardness values were registered at the HAZ-F near to LF-F due to Martensite formation and the highest microhardness values were on GA specimen, as a result of the bigger heat input during the welding process. Microhardness profiles of GA and GB specimens are quite similar, regardless of welding process parameters, moreover, after immersion corrosion tests, the microhardness profiles showed a slight variation of ~1 % at HAZ in both specimens, a fact attributed to microstructure damage caused by pitting and intergranular corrosion. Similar results have been reported by other researchers [16, 37].

Figure 10 illustrates the predicted microstructure of the fusion zone corresponding to 43 % of dilution and Chromium and nickel equivalent of 22, 3 and 11,8 respectively. The microstructure of the fusion zone is composed of 84 % of austenite and 16 % of ferrite and its Creq/Nieq ratio is 1.9, a low and common ratio on austenitic stainless steels. Low Creq/Nieq ratios mean low susceptibility to develop welding metallurgical defects. Also, the low content of ferrite decreases hot and cold cracking, embrittlement, grain growth, and sigma phase formation [12,18, 38], consequently, it is expected a high corrosion resistance in the fusion zone. It is worth mentioning that mechanisms and mode of solidification were not considered in this analysis.

Figure 11 shows Sy, UTS, and ε% of AISI 316L, AISI 430, and GA and GB specimens before (non-immersed condition - NI) and after corrosion immersion. Mechanical properties of AISI 316L and AISI 430 correspond to the annealed condition of these steels, as reported in other works [39, 40].

UTS of GA and GB specimens in all conditions exhibited statistically similar results to those of AISI 430 in as-received condition despite corrosion damage, moreover, the failure of all specimens was in AISI 430 side, suggesting that the welding process did not modify significantly UTS of metal bases, and interesting fact to

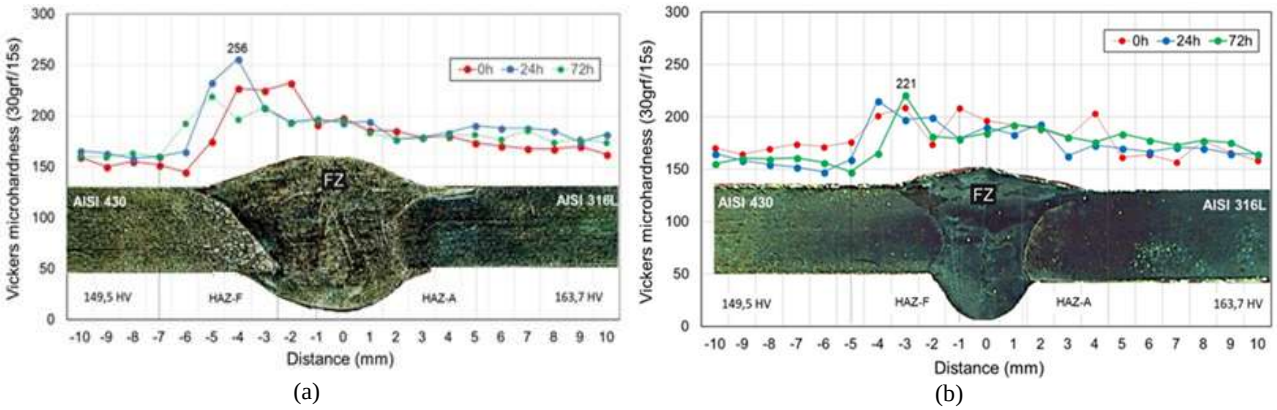

(a) (b)

Figure 9. Vickers microhardness profile along the cross-section of welded joints specimens before and after immersion tests. (a) GA specimen, and (b) GB specimen

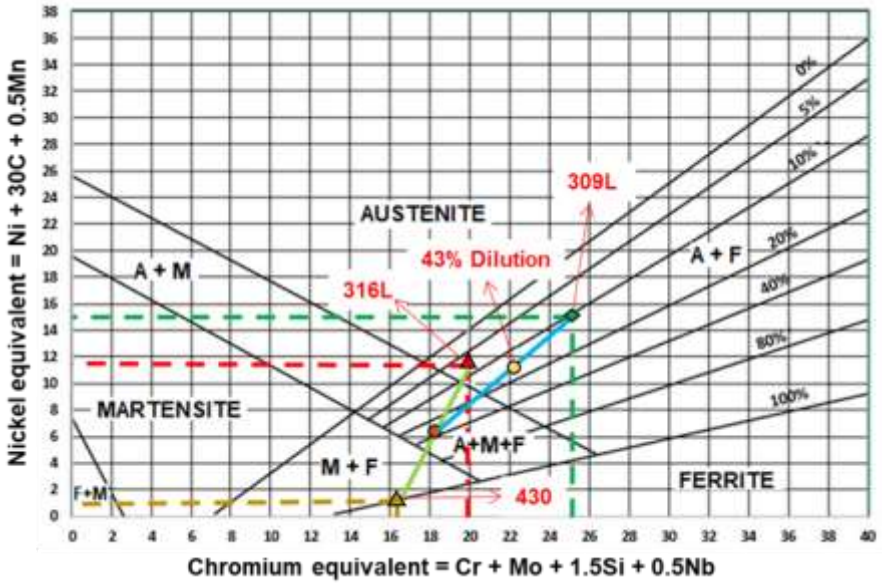

Figure 10. Schaeffler diagram illustrating the predicted microstructure of fusion zone corresponding to 43 % of dilution and Chromium and nickel equivalent of 22.3 and 11.8 respectively. 309L, 316L, and 430 are corresponding to AISI 309L, AISI 316L and AISI 430 stainless steels.

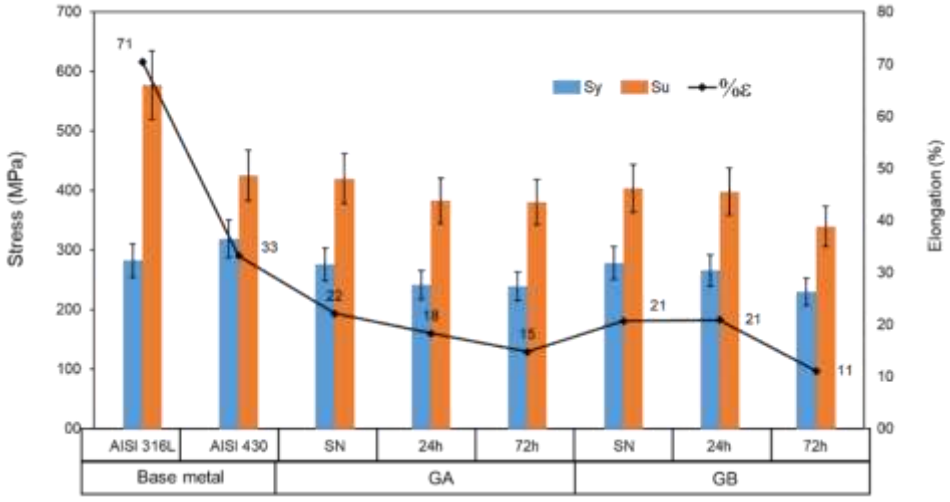

Figure 11. Yield Strength (Sy), Ultimate Tensile Strength (UTS), and Elongation Percentage (ε%) calculated from stress-strain diagrams

consider for mechanical design. In contrast, Sy and ε% decreased with immersion time, particularly the latter at 72 hours of immersion time. ε% reduction is a consequence of Martensite formation and coarsening of ferrite grains at HAZ-F, features that deteriorate ductility of welded joints [41, 42]. Furthermore, Sy and ε% were lower on GB specimens compared to GA specimens, which is attributed to heat input differences. Lower heat input on GB specimen was accomplished by a combination of welding parameters and shielding gas mixtures, including oxygen with lower ionization energy compared to argon and helium. Consequently, on HAZ-F of GB specimen, a narrower region containing coarsened ferrite grains and Martensite was formed. As shown before, HAZ-F suffered higher corrosion damage. Pitting and intergranular corrosion were nucleation sites for tensile failure and decreased the effective area of specimens, therefore, a reduction in mechanical properties is expected.

ANOVA results for Sy and UTS as a function of immersion time and shielding gas type are shown in Tables 4 and 5. Independence of variables and homoscedasticity were satisfactorily fulfilled.

TABLE 4. ANOVA results for Sy - Classical sum of squares – type II

Source	Sum of squares	Degree of freedom	Mean square	F- Values	*p*-value (Prob. > F)
Model	5738.37	5	1147.67	4.18	0.0155
X – immersion time	3440.42	2	1720.21	6.27	0.0114
Y – Shielding gas type	7.20	1	7.20	0.026	0.8736
XY	2290.75	2	1145.38	4.18	0.0378
Pure error	3839.66	14	274.26		
Cor. Total	9578.03	19			

TABLE 5. ANOVA results for UTS - Classical sum of squares – type II

Source	Sum of squares	Degree of freedom	Mean square	F- Values	*p*-value (Prob. > F)
Model	12145.35	5	2429.07	5.12	0.0071
X – immersion time	6448.48	2	3224.24	6.79	0.0087
Y – Shielding gas type	1454.86	1	1454.86	3.07	0.1018
XY	4242.02	2	2121.01	4.47	0.0315
Pure error	6643.94	14	474.57		
Cor. Total	18789.30	19			

According to the ANOVA results, the immersion time (X source) and the combination of immersion time and shielding gas type (XY source) are the most influencing factors on Sy and UTS due to their p-values are lower than the probability of error. These results are coherent with the Sy reduction of the specimens with the augment of immersion time which is shown in Figure 11.

4. CONCLUSIONS

Dissimilar welded joints of AISI 430 and AISI 316L stainless steels free of weld defects were produced by the GMAW process using two different shielding gas mixtures. The comclusions can be summarized as follows:

1. Coarsening of ferrite grains and the presence of acicular ferrite and martensite were observed on the heat-affected zone on AISI 430 stainless steel side. In contrast, neither refinement nor coarsening of grains were evident on the heat-affected zone on AISI 316L stainless steel side.
2. The heat-affected zone on AISI 430 stainless steel side suffered higher corrosion damage. It was observed pitting and intergranular corrosion and the damage increased with immersion time.
3. UTS of dissimilar welded joint specimens in all conditions exhibited statistically similar results to those of AISI 430 in the as-received condition, despite corrosion damage. However, Sy and ε% decreased with immersion time, particularly the latter at 72 h of immersion time, due to coarsened ferrite grains, acicular ferrite, martensite, and corrosion damage on the heat-affected zone on AISI 430 stainless steel side.
4. According to the p-value, the immersion time is the most influencing factor on Sy and UTS of the dissimilar welded joints.

5. ACKNOWLEDGMENTS

The authors acknowledge the financial support of Universidad de Cordoba and Universidad Autónoma del Caribe. Likewise, the authors are grateful to Dr. J. F. Santa for his contributions and the scanning electron microscopy characterization.

6. REFERENCES

1. Tabuchi, M., Hongo, H., Abe, F. "Creep strength of dissimilar welded joints using high B-9Cr steel for advanced USC boiler", ***Metallurgical and Materials Transactions A,*** Vol. 45, No. 11, (2014), 5068-5075. DOI: 10.1007/s11661-014-2471-2
2. Lundin, C. D. "Dissimilar metal welds-transition joints literature review", ***Welding Journal,*** Vol. 61, No. 2, (1982), 58-63. http://files.aws.org/wj/supplement/WJ_1982_02_s58.pdf
3. Verma, J., Taiwade, R. V., Khatirkar, R. K., Kumar, A. "A comparative study on the effect of electrode on microstructure and mechanical properties of dissimilar welds of 2205 austeno-ferritic and 316L austenitic stainless steel". ***Materials Transactions,*** Vol. 57, No. 4, (2016), 494-500. DOI: 10.2320/matertrans.M2015321

4. Marashi, P., Pouranvari, M., Amirabdollahian, S., Abedi, A., Goodarzi, M. "Microstructure and failure behavior of dissimilar resistance spot welds between low carbon galvanized and austenitic stainless steels", ***Materials Science and Engineering: A,*** Vol. 480, No. 1-2, (2008), 175-180. DOI: https://doi.org/10.1016/j.msea.2007.07.007
5. Zarooni, M., "Effect of Welding Heat Input on the Intermetallic Compound Layer and Mechanical Properties in Arc Welding-brazing Dissimilar Joining of Aluminum Alloy to Galvanized Steel", ***International Journal of Engineering, Transactions B: Applications,*** Vol. 29, No. 5, (2016), 669-676. DOI: 10.5829/idosi.ije.2016.29.05b.11
6. Shah, L. H., Ishak, M. "Review of research progress on aluminum–steel dissimilar welding", ***Materials and Manufacturing Processes,*** Vol. 29, No. 8, (2014), 928-933. DOI: 10.1080/10426914.2014.880461
7. Ma, Q. H., Wang, S. G., Zhang, L., Li, Y. "Review of Dissimilar Metal Welding Between Duplex Stainless Steel and Carbon Steel [J]". ***Welded Pipe and Tube,*** Vol. 8. (2009).
8. Naffakh, H., Shamanian, M., Ashrafizadeh, F. "Dissimilar welding of AISI 310 austenitic stainless steel to nickel-based alloy Inconel 657", ***Journal of materials processing technology,*** Vol. 209, No. 7, (2009), 3628-3639. DOI: 0.1016/j.jmatprotec.2008.08.019
9. Rathod, D. W., Singh, P. K., Pandey, S., Aravindan, S. "Effect of buffer-layered buttering on microstructure and mechanical properties of dissimilar metal weld joints for nuclear plant application", ***Materials Science and Engineering: A,*** Vol. 666, (2016), 100-113. DOI: 10.1016/j.msea.2016.04.053
10. Joshi, J. R., Potta, M., Adepu, K., Gankidi, M. R., Katta, R. K. "Influence of welding techniques on heat affected zone softening of dissimilar metal maraging steel and high strength low alloy steel gas tungsten arc weldments", ***Transactions of the Indian Institute of Metals,*** Vol. 70, No. 1, (2017), 69-81. DOI: 10.1007/s12666-016-0861-4
11. Mehta, K. (ed.) "Advanced joining and welding techniques: an overview", ***Advanced Manufacturing Technologies,*** 101-136. Springer International Publishing, (2017). DOI: 10.1007/978-3-319-56099-1_5
12. Samal, M. K., Seidenfuss, M., Roos, E., Balani, K. "Investigation of failure behavior of ferritic–austenitic type of dissimilar steel welded joints", ***Engineering Failure Analysis,*** Vol. 18, No. 3, (2011), 999-1008. DOI: 10.1016/j.engfailanal.2010.12.011
13. Rahmani, M., Eghlimi, A., Shamanian, M. "Evaluation of microstructure and mechanical properties in dissimilar austenitic/super duplex stainless steel joint". ***Journal of Materials Engineering and Performance,*** Vol. 23, No. 10, (2014), 3745-3753. DOI: 10.1007/s11665-014-1136-z
14. Ghasemi, R., Beidokhti, B., Fazel-Najafabadi, M. "Effect of delta ferrite on the mechanical properties of dissimilar ferritic-austenitic stainless steel welds", ***Archives of Metallurgy and Materials,*** Vol. 63, No. 1, (2018), 437-443. DOI: 10.24425/118958
15. Rajput, S. K., Kumar, A., Tripathi, S. S., Sachan, E. "Investigation of microstructural behavior and mechanical properties of dissimilar weld joints of austenitic-ferritic stainless steel", ***Materials Today: Proceedings***, Vol. 25, (2020), 778-784. DOI: 10.1016/j.matpr.2019.09.018
16. Aguilar, S.; Tabares, R.; Serna, C. "Microstructural transformations of dissimilar austenite-ferrite stainless steels welded joints.", ***Journal of Materials and Physical Chemistry,*** Vol. 1, No. 4, (2013), 65-68. DOI: 10.12691/jmpc-1-4-2
17. Paul, V. T., Karthikeyan, T., Dasgupta, A., Sudha, C., Hajra, R. N., Albert, S. K., S. Saroja and Jayakumar, T. "Microstructural variations across a dissimilar 316L austenitic: 9Cr reduced activation ferritic martensitic steel weld joint", ***Metallurgical and Materials Transactions A,*** Vol. 47, No. 3, (2016), 1153-1168. DOI: 10.1007/s11661-015-3281-x
18. DuPont, J. N. "Microstructural evolution and high temperature failure of ferritic to austenitic dissimilar welds", ***International Materials Reviews,*** Vol. 57, No. 4, (2012), 208-234. DOI: 10.1179/1743280412Y.0000000006
19. Hastuty, S., Nishikata, A., Tsuru, T. "Pitting corrosion of Type 430 stainless steel under chloride solution droplet", ***Corrosion Science,*** Vol. 52, No. 6, (2010), 2035-2043. DOI: 10.1016/j.corsci.2010.02.031
20. Wang, C., Yu, Y., Yu, J., Zhang, Y., Zhao, Y., Yuan, Q. (2020). "Microstructure evolution and corrosion behavior of dissimilar 304/430 stainless steel welded joints", ***Journal of Manufacturing Processes***, Vol. 50, (2020), 183-191. DOI: 10.1016/j.jmapro.2019.12.01
21. Nishimura, R., Maeda, Y. "Metal dissolution and maximum stress during SCC process of ferritic (type 430) and austenitic (type 304 and type 316) stainless steels in acidic chloride solutions under constant applied stress", ***Corrosion Science***, Vol. 46, No. 3, (2004), 755-768. DOI: 10.1016/j.corsci.2003.07.002
22. Li, C. X., Bell, T. "Corrosion properties of plasma nitrided AISI 410 martensitic stainless steel in 3.5% NaCl and 1% HCl aqueous solutions", ***Corrosion Science,*** Vol. 48, No. 8, (2006), 2036-2049. DOI: 10.1016/j.corsci.2005.08.011
23. Ethiraj, N., Sivabalan, T., Sivakumar, B., Vignesh Amar, S., Vengadeswaran, N., Vetrivel, K. Effect of Tool Rotational Speed on the Tensile and Microstructural Properties of Friction Stir Welded Different Grades of Stainless Steel Joints. ***International Journal of Engineering, Transactions A: Basics,*** Vol. 33, No. 1, (2020), 141-147. DOI: 10.5829/ije.2020.33.01a.16
24. Maheswara G. U., Srinivasa Ch. "Investigation of Pitting Corrosion Rate on Micro Plasma Arc Welded Dissimilar Weld Joints of AISI 304 and AISI 430 Stainless Steel Sheets", ***ADMT Journal***, Vol. 13, No. 3, (2020), 59-66. DOI: 10.30495/admt.2020.1898623.1195
25. Ranjbari, G., and Doniavi, A. "Prediction and optimization of mechanical properties of st52 in gas metal arc weld using response surface methodology and anova", ***International Journal of Engineering, Transactions C: Aspects,*** Vol. 29, No. 9, (2016), 1307-1313. DOI: 10.5829/idosi.ije.2016.29.09c.17
26. Ghaderi, A, Bani Mostafa Arab, N., Sheikhi, M. M., Nikoi, R., and Arham Nmazi, A. "Experimental Analysis of Effects of Ultrasonic Welding on Weld Strength of Polypropylene Composite Samples", ***International Journal of Engineering, Transactions C: Aspects,*** Vol. 28, No. 3, (2015), 447-53. DOI: 10.5829/idosi.ije.2015.28.03c.15
27. Davis, J. R. (Ed.). (1994). Stainless steels. ASM international.
28. AWS A5.9/A5.9M, 9th Edition, 2017 - Welding Consumables-Wire Electrodes, Strip Electrodes, Wires, and Rods for Arc Welding of Stainless and Heat Resisting Steels- Classification
29. ASTM E407-07(2015)e1, Standard Practice for Microetching Metals and Alloys, ASTM International, West Conshohocken, PA, 2015, www.astm.org DOI: 10.1520/E0407-07R15E01
30. ASTM E384-17, Standard Test Method for Microindentation Hardness of Materials, ASTM International, West Conshohocken, PA, 2017, www.astm.org DOI: 10.1520/E0384-17
31. ASTM E8 / E8M-21, Standard Test Methods for Tension Testing of Metallic Materials, ASTM International, West Conshohocken, PA, 2021, www.astm.org DOI: 10.1520/E0008_E0008M-21
32. ASTM A262-02, Standard Practices for Detecting Susceptibility to Intergranular Attack in Austenitic Stainless Steels, ASTM International, West Conshohocken, PA, 2002, www.astm.org DOI: 10.1520/A0262-02

33. Gupta S. K., Raja A. R., Vashista M. and Yusufzai M. Z. K., "Effect of heat input on microstructure and mechanical properties in gas metal arc welding of ferritic stainless steel", ***Materials Research Express,*** Vol. 6, No. 3, (2018), 036516. DOI: 10.1088/2053-1591/aaf492
34. Saha S., Mukherjee M. and Kumar T., "Microstructure, Texture, and Mechanical Property Analysis of Gas Metal Arc Welded AISI 304 Austenitic Stainless Steel", ***Journal of Materials Engineering and Performance***, Vol. 24, No. 3, (2018), 1125-1139. DOI: 10.1007/s11665-014-1374-0
35. Mukherjee M. and Pal T., "Influence of Heat Input on Martensite Formation and Impact Property of Ferritic-Austenitic Dissimilar Weld Metals", ***Journal of Materials Science & Technology***, Vol. 28, No. 4, (2012), 343-352. DOI: 10.1016/S1005-0302(12)60066-8
36. Bogaard, R. H. "Thermal conductivity of selected stainless steels". ***Thermal Conductivity***, Vol. 18, (1985), 175-185. DOI: 10.1007/978-1-4684-4916-7_20
37. Olmos, M., Martinez, K., and Unfried, J. "Efecto del ciclo térmico sobre la microestructura de la zona afectada térmicamente de juntas soldadas de aceros inoxidables disímiles obtenidas por el proceso SMAW", in XII International Conference–Latin American and Caribbean Consortium of Engineering Institutions-LACCEI. Guayaquil, Ecuador, (2014).
38. Teker T. and Kursun T., "Effect of the manual (GMAW) and pulsed (P-GMAW) welding processes on impact strength and fracture behavior of AISI 304-AISI 1040 dissimilar steel joints fabricated by ASP316L austenitic stainless steel filler metal", ***Kovove materialy - Metallic Materials***, Vol. 55, No. 2, (2017), 141-148. DOI: 10.4149/km_2017_2_141
39. Kheiri, S., Mirzadeh, H., and Naghizadeh, M. "Tailoring the microstructure and mechanical properties of AISI 316L austenitic stainless steel via cold rolling and reversion annealing", ***Materials Science and Engineering: A***, Vol. 759, (2019), 90-96. DOI: 10.1016/j.msea.2019.05.028
40. Tavares, S., Souza, L., Chuvas, C., Machado, C., and Almeida, C. "Influence of heat treatments on the microstructure and degree of sensitization of base metal and weld of AISI 430 stainless steel", ***Matéria*** (Rio de Janeiro), Vol. 22, No. 1, (2017). DOI: 10.1590/s1517-707620170005.0275
41. Ghosh, N., Pal, P. K., and Nandi, G." GMAW dissimilar welding of AISI 409 ferritic stainless steel to AISI 316L austenitic stainless steel by using AISI 308 filler wire", ***Engineering Science and Technology, an International Journal***, Vol. 20, No. 4, (2017), 1334-1341. DOI: 10.1016/j.jestch.2017.08.002
42. Pańcikiewicz, K., Świerczyńska, A., Hućko, P., and Tumidajewicz, M. "Laser dissimilar welding of AISI 430F and AISI 304 stainless steels", ***Materials***, Vol. 13, No. 20, (2020), 4540. DOI: 10.3390/ma13204540

Persian Abstract

چکیده

اتصالات جوش داده شده غیر مشابه فولاد ضد زنگ AISI 430 و AISI 316L توسط فرآیند GMAW با استفاده از دو مخلوط مختلف گاز محافظ متشکل از Ar-۹۷ 3N2 و Ar-19He-1O2۸۰ تولید شده است. ریزساختار منطقه تحت تأثیر گرما توسط میکروسکوپ الکترونی نوری و روبشی مشخص شد و اندازه گیری های سختی ویکرز در سطح مقطع نمونه ها انجام شد. اتصالات جوش داده شده غیرمشابه به مدت ۲۴ و ۷۲ ساعت به آزمایش خوردگی غوطه وری در محلول اسید کلریدریک ۱۰٪ (v/v) ارسال شد. پس از آن ، استحکام بازده ، مقاومت کششی و درصد کشیدگی با استفاده از آزمون های کششی مطابق با استاندارد ASTM E8 اندازه گیری شد. برای مقایسه از اتصالات جوشکاری نشده غوطه ور استفاده شد. تجزیه و تحلیل واریانس برای ارزیابی تأثیر زمان غوطه وری و مخلوط گاز محافظ بر مقاومت در برابر مقاومت و مقاومت در برابر کشش ایجاد شد. خصوصیات ریزساختار نشان داد که منطقه تحت تأثیر گرما در سمت AISI 430 وسیع ترین بوده و وجود چشمگیر دانه های فریتی ، مارتنزیت و دانه درشت مشاهده شده است. در مقابل ، در منطقه تحت تأثیر گرما در سمت AISI 316L درشت و تصفیه دانه های آستنیت مشاهده نشد. منطقه تحت تأثیر گرما AISI 430 حداکثر مقادیر سختی و حساسیت بیشتر به آسیب خوردگی را نشان داد. نتایج آزمون های کششی نشان داد که آزمون های خوردگی غوطه وری در مقایسه با نمونه های غیر غوطه وری مقاومت نهایی به طور قابل توجهی تغییر نمی کند در حالی که به دلیل زمان غوطه وری مقاومت و بازده عملکرد به شدت کاهش می یابد. با توجه به مقدار p ، زمان غوطه وری بیشترین عامل تأثیر در مقاومت در برابر بازده و مقاومت کششی اتصالات جوش داده شده غیر مشابه دارد.